

Technical Note

Radiotherapy planning of spine and pelvis using single-energy metal artifact reduction corrected computed tomography sets



Daliya Ignatius^{a,1,*}, Zaid Alkhatib^b, Pejman Rowshanfarzad^{a,2}, Simon Goodall^{a,4}, Mounir Ibrahim^b, Andrew Hirst^{a,5}, Riley Croxford^a, Joshua Dass^b, Mahsheed Sabet^{a,b,3}

^a School of Physics, Mathematics and Computing, The University of Western Australia, Crawley, WA, Australia

^b Department of Radiation Oncology, Sir Charles Gairdner Hospital, Nedlands, WA, Australia

ARTICLE INFO

Keywords:

Single-Energy Metal Artifact Reduction (SEMAR)
Metal artifacts
Computed Tomography (CT)
Radiotherapy treatment planning
3D printing

ABSTRACT

Metal artifacts produce incorrect Hounsfield units and impact treatment planning accuracy. This work evaluates the use of single-energy metal artifact reduction (SEMAR) algorithm for treatment planning by comparison to manual artifact overriding. CT datasets of in-house 3D-printed spine and pelvic phantoms with and without metal insert(s) and two treated patients with metal implants were analysed. CT number accuracy improved with the use of SEMAR filter: root mean square deviation (RMSD) from reference (without metal) reduced by 35.4 in spine and 98.8 in hip. The plan dose volume histograms (DVHs) and dosimetric measurements showed comparable results. SEMAR reconstruction improved planning efficiency.

1. Introduction

In external beam radiation therapy (EBRT), acquisition of computed tomography (CT) images of patients allows for the delineation of the target volumes and organs at risk[1]. CT scans of patients with metal implants can contain errors during reconstruction in the form of bright and/or dark streaking metal artifacts[2]. These artifacts affect contouring and CT numbers in Hounsfield units (HU), which can result in incorrect relative electron densities (RED) and subsequent dose calculation errors[3]. Hence, an improvement in CT numbers is expected to improve the dose calculation accuracy[4]. To eliminate the effect of metal artifacts on treatment planning, the artifact-affected areas are usually overridden with a suitable density. However, this traditional method has limitations, including the need for artifacts to be manually contoured on individual CT slices which is time consuming and labour intensive, therefore increasing the associated costs, and may introduce some level of subjectivity which could increase the uncertainties in dose calculation[5]. Forcing density to artifact-affected areas may become more concerning when the metal is inside or close to the planning target

volume (PTV) due to difficulty of outlining and inaccuracies in the assigned CT numbers.

Single-energy metal artifact reduction (SEMAR, Canon Medical Systems Corporation, Otawara, Japan) is one of the many commercially available clinically used metal artifact reduction techniques[6]. SEMAR has proved to reduce metal artifacts in a range of clinical sites[7–11]. There are reports in the literature on improvements in CT number prediction and dose calculation accuracy by using SEMAR in carbon-ion therapy [12], brachytherapy[13], and EBRT[4]. The study on EBRT acknowledged two limitations of their work: the densities of regions with artifacts were not overridden for dose calculation, and the results were not compared to measured doses[4].

Since EBRT treatment plans are never created on raw CT sets with metal artifacts, this study aims to evaluate the accuracy of using SEMAR-corrected CT sets for EBRT planning through comparisons with the traditional method of artifact overrides in patients with metal implants in spine and pelvic regions. Various aspects have been considered, including CT number accuracy, retrospective planning studies on previously treated patients, and dosimetry measurements in phantoms.

* Corresponding author.

E-mail addresses: daliya.ignatius@health.nsw.gov.au, 22751416@student.uwa.edu.au (D. Ignatius).

¹ Daliya Ignatius: 0000-0002-3219-2719.

² Pejman Rowshanfarzad: 0000-0001-8306-7742.

³ Mahsheed Sabet: 0000-0003-1050-0749.

⁴ Simon Goodall: 0000-0003-3318-9703.

⁵ Andrew Hirst: 0000-0002-4050-0777.

2. Methods

2.1. Phantom design and printing

2.1.1. Spine phantom

Two in-house 3D printed spine phantoms constructed by Goodall et al. [14] were used in this study. The phantom (Supplementary Fig. 1a) had eight modules, including: three polylactic acid (PLA) only “body” modules, four dual printed StoneFil-Concrete “spine” modules, and one dual ionization chamber holder. The body of the phantom was composed of one anterior module and two mirrored left and right components with areas of 0.3 mm depth on the face of each module to accommodate Gafchromic EBT3 film (Ashland Advanced Materials, NY, USA). One pair of the spine modules was designed without metal inserts, and another pair to hold two titanium screws bilaterally of length 50 mm, diameter 7 mm, and head diameter 12.3 mm as shown in Supplementary Fig. 1c. More information about the design and printing of this phantom is reported by Goodall et al. [14].

2.1.2. Hip phantom

Two hip phantoms were fabricated in-house using 3D printing: one without metal and the other with a titanium rod of diameter 31.4 mm and length 110.0 mm inserted into one of its femoral head replicating a unilateral hip implant (brief explanation on the hip phantom construction is in the Supplementary Materials). The femoral heads were constructed with an attachment to hold a CC04 ionization chamber (IBA).

2.2. Data acquisition

All phantoms were CT scanned using a 16-slice large bore CT scanner (Aquilion ONE; Canon Medical Systems, Otawara, Japan) with 120 kV_p, effective mAs: 312, pitch: 1.5, resolution: 1.07 mm, and slice thickness: 2 mm. The hip phantom was scanned with a CC04 chamber inserted. Three datasets were obtained for each phantom: one corresponding to phantoms without metal, CT_{Ref}, and the other two corresponding to phantoms with metal which were reconstructed with and without the application of SEMAR filter, CT_{SEMAR} and CT_{No_SEMAR}, respectively.

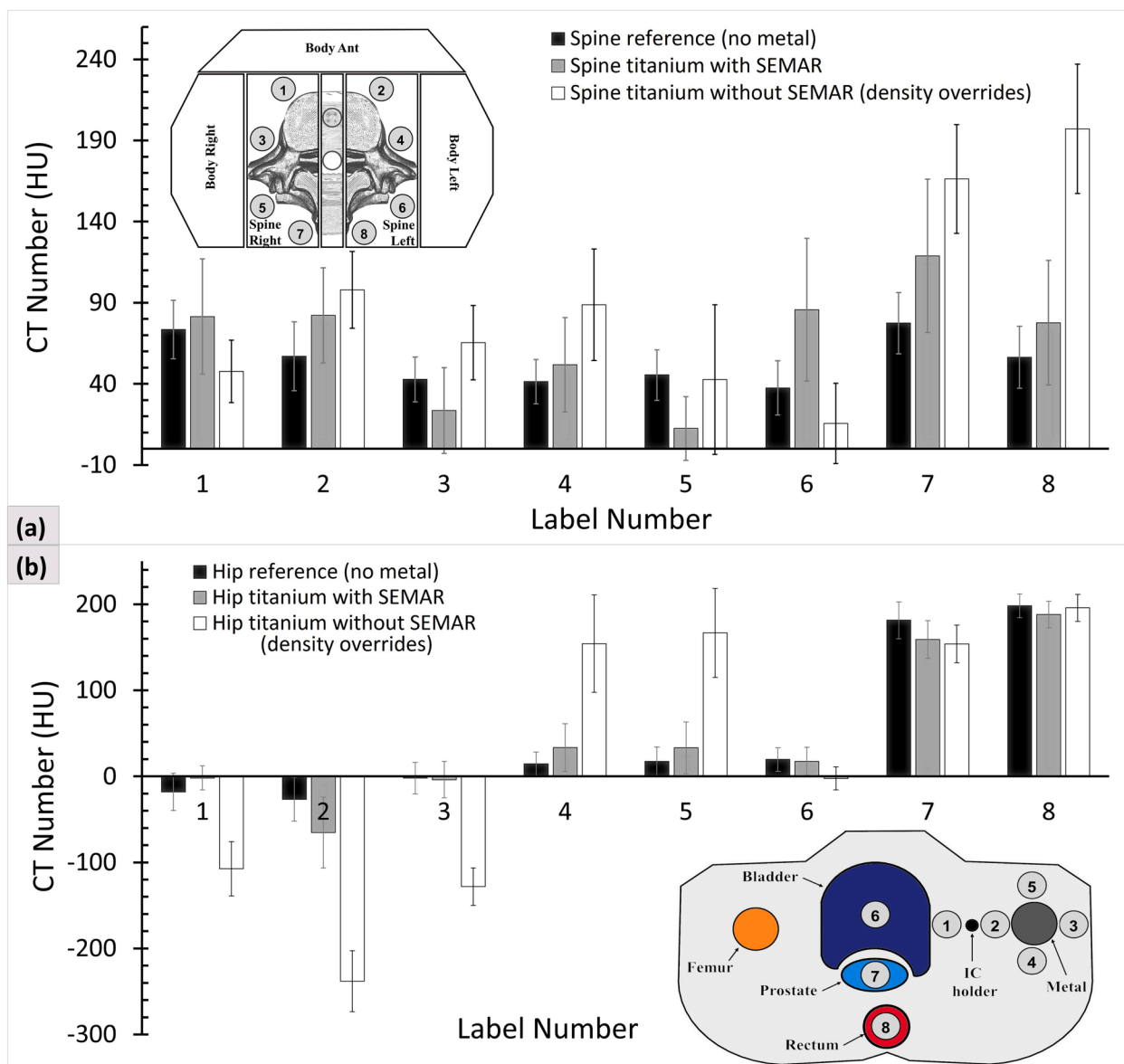


Fig. 1. CT numbers for eight VOIs in (a) the spine phantom (avoiding the titanium screws) and (b) the hip phantom, as shown on the labelled schematic of the phantom.

2.3. CT number accuracy

For each phantom, five most artifact-affected contiguous slices were selected and the corresponding slices to the same position on both phantoms were investigated on the three datasets (CT_{Ref}, CT_{SEMAR}, and CT_{No_SEMAR}). Multiple slices were selected to reduce uncertainties in the average CT number to within acceptable limits. For each dataset, eight cylindrical volumes of interest (VOIs) were drawn on the selected slices avoiding the metal inserts (Fig. 1) in ImageJ software (NIH, Maryland, USA)[15]. The CT numbers for each VOI for all three datasets were recorded and differences were quantified using the root mean square deviation (RMSD).

2.4. Planning studies

For each type of phantom, dose on the CT dataset with metal was calculated under two different artifact reduction techniques: artifacts on the CT_{No_SEMAR} dataset were manually outlined and overridden with RED of soft tissue, and for the CT_{SEMAR} dataset, artifact reduction was performed using the SEMAR filter function. All relevant structures including the PTV and OARs were then contoured. For each type of phantom, a clinically approved VMAT treatment plan was copied to the CT_{SEMAR} and CT_{No_SEMAR} datasets. Dose was then calculated with the same number of monitor units and MLC segmentation. Dose predictions on CT_{SEMAR} were compared to those on CT_{No_SEMAR} using DVH analysis.

Two CT datasets from previously treated patients were selected for the retrospective study: Patient-1 with unilateral hip implant and Patient-2 with bilateral hip implants. The ethics approval for this project was granted by the Sir Charles Gairdner Osborne Park Hospital Group as a Quality Improvement Activity (44054). The original clinical plans were calculated with artifacts contoured and manually overridden. In this study, these datasets were reconstructed with SEMAR filter applied, and the clinically used treatment plans were recalculated on the SEMAR-corrected CT sets. The predicted doses on plans were compared using DVH analysis.

All dose calculations were performed using Acuros XB (AXB) algorithm version 15.6 with dose to medium approach on Eclipse treatment planning system (TPS) version 13.6.30 (Varian Medical Systems, Palo Alto, CA, USA).

2.5. Dosimetry measurements

To further investigate the dose calculation accuracy, measurements were made in the phantoms with metal inserts, using Gafchromic EBT3 film in the spine phantom and ionisation chamber in the hip phantom. The calculated plans were delivered to the phantoms on a linear accelerator (TrueBeam™, Varian Medical System Inc., Palo Alto, CA, USA).

The film measured doses in the spine phantom with titanium screws (CT_{Spine_SEMAR} and CT_{Spine_No_SEMAR}) were compared with that in the reference phantom (CT_{Spine_Ref}) in the same plane. 2D Gamma analysis was performed using SNC Patient software (version 6.7.3; Sun Nuclear Corporation, FL, USA).

On the hip phantom, point dose measurement was performed using a cross-calibrated CC04 chamber inserted into a holder attached to the titanium rod. The measurement was repeated three times and the average was used for comparison to the TPS-calculated doses at the same point on the CT_{Hip_SEMAR} and CT_{Hip_No_SEMAR} datasets.

3. Results

3.1. CT number accuracy

As expected, the streaking artifacts on the CT images of phantoms with metal inserts were visibly reduced after applying the SEMAR filter (Supplementary Fig. 3), which in turn improved the CT numbers (Fig. 1).

For the spine phantom, the mean CT number of the eight VOIs was

53.9 ± 17.3 HU on CT_{Spine_Ref}, 66.7 ± 34.8 HU on CT_{Spine_SEMAR}, and 90.2 ± 31.8 HU on CT_{Spine_No_SEMAR}. The RMSD was 29.1 between CT_{Spine_Ref} and CT_{Spine_SEMAR}, and 64.5 between CT_{Spine_Ref} and CT_{Spine_No_SEMAR}.

For the hip phantom, the mean CT number of the eight VOIs was 48.0 ± 18.6 HU on CT_{Hip_Ref}, 45.0 ± 25.0 HU on CT_{Hip_SEMAR}, and 24.3 ± 34.5 HU on CT_{Hip_No_SEMAR}. The RMSD was 19.3 between CT_{Hip_Ref} and CT_{Hip_SEMAR}, and 118.1 between CT_{Hip_Ref} and CT_{Hip_No_SEMAR}.

3.2. Planning studies

Treatment plans and DVHs for the spine and hip phantoms are shown in Supplementary Fig. 4 and Fig. 2a, respectively. The PTV-D₅₀ for CT_{Spine_SEMAR} and CT_{Spine_No_SEMAR} were 50.03 Gy and 49.94 Gy, respectively, while that for CT_{Hip_SEMAR} and CT_{Hip_No_SEMAR} were 46.12 Gy and 46.04 Gy, respectively.

The plans and DVHs for Patient-1 and Patient-2 are shown in Fig. 2 b and c, respectively. The PTV-D₅₀ for CT_{Pt1_SEMAR} and CT_{Pt1_No_SEMAR} were 54.39 Gy and 54.56 Gy, respectively, while that for CT_{Pt2_SEMAR} and CT_{Pt2_No_SEMAR} were 79.17 Gy and 79.16 Gy, respectively.

3.3. Dosimetry measurements

Supplementary Fig. 5 shows the 2D gamma analysis comparing the film-measured dose distribution for CT_{Spine_SEMAR} and CT_{Spine_No_SEMAR} with that of CT_{Spine_Ref}. The Gamma pass rates for CT_{Spine_SEMAR} and CT_{Spine_No_SEMAR} were 93.7% and 79.7% for the 3%/3 mm criteria.

The measured point dose in the hip phantom was 1.92 Gy, while the calculated point doses on the CT_{Hip_SEMAR} and the CT_{Hip_No_SEMAR} with manual artifact overrides were 1.88 Gy and 1.87 Gy, respectively. Hence, the percentage dose differences with measured dose were -2.0% and -2.5% , respectively.

4. Discussion

The present study made a detailed comparison between using the traditional method of manually overriding metal artifacts and using SEMAR-corrected CT scans for EBRT treatment planning of patients with metal implants in spine and pelvis.

SEMAR improved the image quality as expected, although some artifacts persisted. The CT numbers in the vicinity of metal were accurately recovered with SEMAR except for VOIs 5 and 6 in the spine phantom. As detailed in Goodall *et al* [14], the differences seen between the left and the right modules of the spine phantom with titanium can be due to the inherent variation in CT number of 12.0 ± 31.9 HU from phantom construction whereas that between the reference phantom and the one with metal is 25 ± 31.9 HU for the left modules and 47.3 ± 33.3 HU for the right modules. All CT numbers from regions far from the metal were acceptably restored. These findings were in line with previous studies on SEMAR filter [4,12]. The RMSD between CT_{Ref} and CT_{SEMAR} for both phantoms were considerably lower in comparison to that between CT_{Ref} and CT_{No_SEMAR}. The results showed that reconstruction of metal artifact-affected images with SEMAR generated CT numbers closer to the corresponding metal-free CT scan and was therefore more accurate than the traditional method of artifact overrides.

In the DVH analysis, near identical dose distributions with clinically negligible dose differences were observed between the plans on CT_{SEMAR} and CT_{No_SEMAR}. For the spine phantom, the percentage difference in dose distribution between CT_{Spine_SEMAR} and CT_{Spine_No_SEMAR} for PTV-D₅₀ was 0.18%. Similarly, for the hip phantom, the percentage difference in dose distribution between CT_{Hip_SEMAR} and CT_{Hip_No_SEMAR} for PTV-D₅₀ was 0.17%. For the retrospective patient study, PTV-D₅₀ percentage dose differences for CT_{SEMAR} and CT_{No_SEMAR} for Patient-1 was -0.31% , while that for patient-2 was 0.01%. These results indicated that the accuracy of dose calculation is comparable between the two methods. However, although DVH statistics were quite close, the

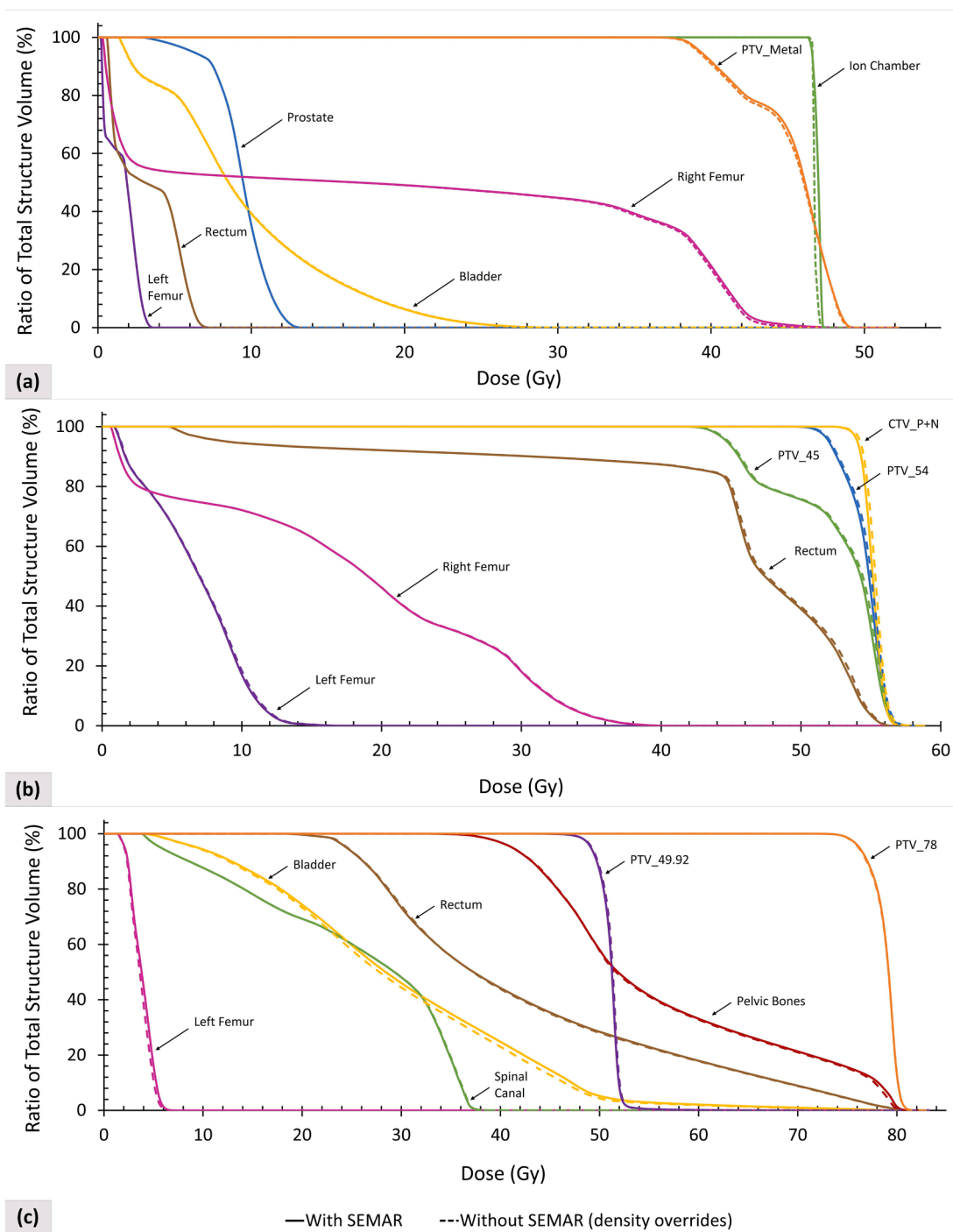


Fig. 2. DVH analysis for (a) hip phantom with PTV including metal comparing CT_{Hip_SEMAR} and $CT_{Hip_No_SEMAR}$ with manual artifact overrides; (b) Patient-1 with unilateral hip implant with PTV in the bladder comparing CT_{P1_SEMAR} and $CT_{P1_No_SEMAR}$; (c) Patient-2 with bilateral hip implants with PTV in the prostate comparing CT_{P2_SEMAR} and $CT_{P2_No_SEMAR}$.

differences noted in CT number accuracy may have significance in adjacent OARs, such as spinal cord tolerance. The other possibility is that the DVH study may not be sufficiently sensitive to detect such differences.

Dosimetric analysis of the spine phantom using film showed higher Gamma pass rates for CT_{Spine_SEMAR} by 14% for the 3%/3 mm criteria. Similarly, for the hip phantom, the measured point dose was closer to the planned dose on CT_{Hip_SEMAR} by 0.5%. The difference although small and clinically insignificant confirmed that using SEMAR for treatment planning was dosimetrically comparable (if not more accurate) to the

traditional method of overriding the density of artefact-affected areas.

Ideally, it would have been quite useful to compare the performance of all the metal artefact reduction techniques used by different manufacturers but due to time limits and Covid-19 restrictions it became practically impossible to arrange with multiple radiotherapy sites.

Results of this study showed that incorporation of SEMAR into EBRT treatment planning workflow can save a lot of effort and time in contouring and avoid subjectivity in overriding artifacts without compromising dosimetric accuracy.

Declaration of Competing Interest

The authors declare that they have no known competing financial interests or personal relationships that could have appeared to influence the work reported in this paper.

Acknowledgements

The authors would like to extend appreciation to the medical physics team in Sir Charles Gardiner Hospital, GenesisCare Cancer Center WA, University of Western Australia, and ICON Cancer Center WA for their guidance, support, and resources during this study. Special thanks to Brendan James Chick, Mahesh Mundayadan Chandroth, and Anthony James Venning for their insightful review and critique in the drafting of this manuscript. The authors would like to thank Gabor Neveri for advice and help with CT scanning the phantoms.

Informed consent

For this type of study, formal consent was not needed.

Funding

The authors declare that no funds, grants, or other support were received during the preparation of this manuscript.

Appendix A. Supplementary data

Supplementary data to this article can be found online at <https://doi.org/10.1016/j.phro.2023.100449>.

References

- [1] Mutic S, Palta J R, Butker E K, Das I J, Huq M S, Loo, L-N D, et al. Quality assurance for computed-tomography simulators and the computed-tomography-simulation process: report of the AAPM radiation therapy committee task group no. 66. *Med Phys*. 2003;30:2762-2792. doi: 10.1118/1.1609271.
- [2] De Man B, Nuyts J, Dupont P, Marchal G, Suetens P. Metal streak artifacts in x-ray computed tomography: a simulation study. *IEEE Trans Nucl Sci* 1999;46:691-6. <https://doi.org/10.1109/23.775600>.
- [3] Puvanasunthararajah S, Fontanarosa D, Wille M, Camps S. The application of metal artifact reduction methods on computed tomography scans for radiotherapy applications: a literature review. *J Appl Clin Med Phys* 2021;22:198-223. <https://doi.org/10.1002/acm2.13255>.
- [4] Murazaki H, Fukunaga J, T-aki H, Funatsu N, Matsumoto R, Hidaka K, et al. Dosimetric assessment of a single-energy metal artifact reduction algorithm for computed tomography images in radiation therapy. *Radiol Phys Technol* 2019;12: 268-76. <https://doi.org/10.1007/s12194-019-00517-7>.
- [5] Rousselle A, Amelot A, Thariat J, Jacob J, Mercy G, De Marzi L, et al. Metallic implants and CT artefacts in the CTV area: Where are we in 2020? *Cancer Radiother* 2020;24:658-66. <https://doi.org/10.1016/j.canrad.2020.06.022>.
- [6] Kataoka M, Hochman M, Rodriguez E, Lin P, Kubo S, Raptopoulos V. A review of factors that affect artifact from metallic hardware on multi-row detector computed tomography. *Curr Probl Diagn Radiol* 2010;39:125-36. <https://doi.org/10.1067/j.cpradiol.2009.05.002>.
- [7] Kidoh M, Utsunomiya D, Ikeda O, Tamura Y, Oda S, Funama Y, et al. Reduction of metallic coil artifacts in computed tomography body imaging: effects of a new single-energy metal artifact reduction algorithm. *Eur Radiol* 2016;26:1378-86. <https://doi.org/10.1007/s00330-015-3950-6>.
- [8] Niehues S, Vahldiek J, Tröltzsch D, Hamm B, Shnayien S. Impact of single-energy metal artifact reduction on CT image quality in patients with dental hardware. *Comput Biol Med*. 2018;103:161-166. doi: 0.1016/j.combiomed.2018.10.023.
- [9] Sonoda A, Nitta N, Ushio N, Nagatani Y, Okumura N, Otani H, et al. Evaluation of the quality of CT images acquired with the single energy metal artifact reduction (SEMAR) algorithm in patients with hip and dental prostheses and aneurysm embolization coils. *Jpn J Radiol*. 2015;33:717-717. doi: 10.1007/s11604-015-0478-2.
- [10] Sofue K, Yoshikawa T, Ohno Y, Negi N, Inokawa H, Sugihara N, et al. Improved image quality in abdominal CT in patients who underwent treatment for hepatocellular carcinoma with small metal implants using a raw data-based metal artifact reduction algorithm. *Eur Radiol* 2017;27:2978-88. <https://doi.org/10.1007/s00330-016-4660-4>.
- [11] Fang J, Zhang D, Wilcox C, Heidinger B, Raptopoulos V, Brook A, et al. Metal implants on CT: comparison of iterative reconstruction algorithms for reduction of metal artifacts with single energy and spectral CT scanning in a phantom model. *Abdom Radiol* 2017;42:742-8. <https://doi.org/10.1007/s00261-016-1023-1>.
- [12] Miki K, Mori S, Hasegawa A, Naganawa K, Koto M. Single-energy metal artifact reduction with CT for carbon-ion radiation therapy treatment planning. *Br J Radiol* 2016;89:20150988. <https://doi.org/10.1259/bjr.20150988>.
- [13] Shirashi Y, Yamada Y, Tanaka T, Eriguchi T, Nishimura S, Yoshida K, et al. Single-energy metal artifact reduction in postimplant computed tomography for I-125 prostate brachytherapy: impact on seed identification. *Brachytherapy* 2016;15: 768-73. <https://doi.org/10.1016/j.brachy.2016.07.006>.
- [14] Goodall SK, Rampant P, Smith W, Waterhouse D, Rowshanfarzad P, Ebert MA. Investigation of the effects of spinal surgical implants on radiotherapy dosimetry: a study of 3D printed phantoms. *Med Phys* 2021;48:4586-97. <https://doi.org/10.1002/mp.15070>.
- [15] Abramoff M, Magalhães P, Ram SJ. Image Processing with ImageJ. *J Biophotonics*. 2003;11:36-42. https://imagej.nih.gov/ij/docs/pdfs/Image_Processing_with_ImageJ.pdf Accessed September 25, 2021.